Pyun, S., Shin, C., Refraction traveltime tomography using damped monochromatic wavefield.
International Symposium on the Fusion Technology of Geosystem Engineering, Rock Engineering and Geophysical Exploration
Seoul, Korea, Nov. 18-19, 2003

# Refraction traveltime tomography using damped monochromatic wavefield

Sukjoon Pyun, Changsoo Shin
Seoul National University, Seoul, Korea

Abstract: Refraction tomography requires an algorithm for efficiently computing the traveltimes and their Fréchet derivatives. We have attempted to solve the damped wavefield using the frequency domain finite element modeling and then invoked the reciprocity theorem to calculate the Fréchet derivative of the traveltime with respect to the subsurface parameter. Then, we used a damped least square method to invert the traveltimes of the Marmousi-2 model. Numerical tests demonstrate that the refraction tomography with large aperture data can be used to estimate the smooth velocity model for the prestack depth migration.

## 1. Introduction

Refraction survey was originally used to investigate the deep structure of the earth by seismologists in the early twentieth century. Following that, geophysicists were successful in delineating the shallow salt body for oil exploration. With the enhancement of the relevant techniques and the equipments used in conducting reflection survey, such surveying method began to replace refraction survey. Because of the depth penetrating resolution of refracted waves due to limited offset distance from a source to receivers in the reflection seismic survey, refraction survey has been mainly employed to investigate the structure of the shallow subsurface for static correction.

Hampson and Russell(1984) used refraction tomography to compute a multi-layer near-surface model, though the velocity in the weathering layer was assumed to be known. Docherty(1992) have investigated the feasibility of extracting both weathering thickness and velocity information simultaneously, while Landa et al.(1995) have estimated the velocity-depth model by applying the coherence method for the estimation of the shallow subsurface. Landa et al.(1995) have inverted the velocity-depth model in the direction that the semblance coherence could be maximized. Shin et al.(1999) parameterised the subsurface model in blocky and arbitrary shaped layers, and inverted for the velocities and interface coordinates of the geologic model by calculating the Fréchet derivatives of the velocity and the interface coordinate of the blocks.

In this paper, we have proposed a new method for obtaining traveltime and Fréchet derivative by using the monochromatic damped wave solution. For calculating the derivative of the traveltime with respect to the velocity parameter, we exploited the source-receiver reciprocity as Shin et al.(2001) did using the frequency domain modeling technique.

To our knowledge, there has been little study on the issue that the velocity-depth model derived from refraction tomography was used for Kirchhoff prestack depth migration. In this paper, we have applied refraction tomography to Marmousi-2 model(Martin et al., 2002) and built the velocity model that can be used for the initial model of prestack depth migration. The migrated images demonstrate that we can obtain the velocity-depth model suitable for the migration by using the refraction tomography.

## 2. Theory

### Calculation of traveltime and its Fréchet derivative

Shin et al.(2003) introduced a new algorithm for computing the first arrival traveltime by modifying an existing frequency domain modeling technique. Before discussing how to apply their algorithm, we will briefly review their algorithm. When solving the wave equation by using the time domain finite-element method, we need to solve the discretized matrix equation given as

$$\mathbf{M}\ddot{\mathbf{u}} + \mathbf{K}\mathbf{u} = \mathbf{f} \tag{1}$$

where $\mathbf{M}$ is the mass matrix, $\mathbf{K}$ is the stiffness matrix, $\mathbf{u}$ is the solution vector, $\ddot{\mathbf{u}}$ is the second order partial derivative of the solution vector with respect to time, and $\mathbf{f}$ is the source vector(Marfurt, 1984).

In the temporal Fourier domain, we can rewrite equation (1) as

$$\mathbf{S}\tilde{\mathbf{u}} = \tilde{\mathbf{f}} \tag{2}$$

where $\mathbf{S}$ is the complex impedance matrix expressed as

$$\mathbf{S} = \mathbf{K} - \omega^2\mathbf{M} \tag{3}$$

and $\tilde{\mathbf{u}}(\omega)$ and $\tilde{\mathbf{f}}(\omega)$ are the Fourier transforms of $\mathbf{u}(t)$ and $\mathbf{f}(t)$, expressed as

$$\tilde{\mathbf{u}}(\omega) = \int_{-\infty}^{\infty} \mathbf{u}(t)e^{-i\omega t}dt \tag{4}$$

and

$$\tilde{\mathbf{f}}(\omega) = \int_{-\infty}^{\infty} \mathbf{f}(t)e^{-i\omega t}dt\,. \tag{5}$$

In order to obtain the frequency domain wave solution $\tilde{\mathbf{u}}$, we factor the impedance matrix $\mathbf{S}$ into upper and lower triangular matrices. Then we obtain the frequency domain wave solution $\tilde{\mathbf{u}}$ by forward and backward substitutions. In the frequency domain modeling, we often use the complex angular frequency $\omega$ to suppress the wrap around effects.

$$\omega = \omega^* + i\alpha \tag{6}$$

where $\omega^*$ is the real angular frequency and $\alpha$ is the wrap around suppression factor. The resulting wavefield in the time domain is equivalent to the wavefield damped by $e^{-\alpha t}$. By choosing the optimum wrap around suppression factor(Shin et al., 2003), we were able to suppress all the energy following the first arrival and obtain a damped spike.

The damped spike-shaped wavefield is expressed as (Shin et al., 2003)

$$\mathbf{u}(x,y,z,t) = A(x,y,z)e^{-\alpha t}\delta(t-\tau(x,y,z)) \tag{7}$$

where $\mathbf{u}(x,y,z,t)$ is the wavefield in the time domain, $\tau(x,y,z)$ is the traveltime from the source to a depth point in the subsurface, $A(x,y,z)$ is the amplitude at the depth point in the subsurface, and $\delta$ is the Dirac delta function In the frequency domain, we can express equation (7) as

$$\tilde{\mathbf{u}}(x,y,z,t) = Ae^{-\alpha\tau(x,y,z)}e^{i\omega^*\tau(x,y,z)} \tag{8}$$

By taking the logarithm of both sides of equation (8)

$$\ln\tilde{\mathbf{u}}(x,y,z,\omega) = \ln\left|Ae^{-\alpha\tau(x,y,z)}\right| + i\omega^*\tau(x,y,z) \tag{9}$$

Dividing the imaginary component of equation (9) by the real angular frequency $\omega^*$ results in obtaining the traveltime $\tau(x,y,z)$ at each depth point.

By following Shin et al.(2001)'s approach, we calculate the Fréchet derivative wavefield efficiently by applying source-receiver reciprocity to the damped wave equation in the frequency domain and use it for the calculation of the Fréchet derivative of the traveltime of the first arrival event. To proceed, we modify equation (8) as

$$\tilde{u}_{i,j}(\omega) = A_{i,j}e^{-\alpha\tau_{i,j}}e^{i\omega\tau_{i,j}} \tag{10}$$

$$i = 1,2,\cdots,nr\ ;\ j = 1,2,\cdots,ns$$

where $i$ denotes the receiver number, $j$ denotes the shot number, $nr$ is the number of receivers and $ns$ is the number of shots. Following Shin et al.(2001)'s notation, we parameterise our subsurface by an $N = N_x \times N_z$ elements, where $N_x$ is the number of elements in the x-direction and $N_z$ is the number of elements in the z-direction. We, then, identify the velocity at each element. By doing so, we can define our unknown model parameter vector $\mathbf{p}$ to be $\mathbf{p} = [v_1, v_2, \cdots, v_l, \cdots, v_N]$. Then, the wavefield can be expressed as a function of the velocity parameter(Shin, 1988). Thus, we differentiate $\tilde{u}_{i,j}$ with respect to the subsurface velocity parameter $p_l$ to obtain the Fréchet derivative wavefield and express it as

$$\frac{\partial \tilde{u}_{i,j}}{\partial p_l} = \frac{\partial A_{i,j}}{\partial p_l} e^{-\alpha\tau_{i,j}} e^{i\omega\tau_{i,j}} + A_{i,j} e^{-\alpha\tau_{i,j}} (-\alpha) \frac{\partial \tau_{i,j}}{\partial p_l} e^{i\omega\tau_{i,j}} + A_{i,j} e^{-\alpha\tau_{i,j}} e^{i\omega\tau_{i,j}} (i\omega) \frac{\partial \tau_{i,j}}{\partial p_l} \tag{11}$$

$$i = 1,2,\cdots,nr\ ;\ j = 1,2,\cdots,ns\ ;\ l = 1,2,\cdots,N\ .$$

In this stage, we already computed the Fréchet derivative using the reciprocity theorem. Then we continue to use it for the calculation of the Fréchet derivative of the traveltime. Dividing both sides of equation (11) by equation (10) and rearranging it give

$$\frac{1}{\tilde{u}_{i,j}} \frac{\partial \tilde{u}_{i,j}}{\partial p_l} = \frac{1}{A_{i,j}} \frac{\partial A_{i,j}}{\partial p_l} - \alpha \frac{\partial \tau_{i,j}}{\partial p_l} + i\omega \frac{\partial \tau_{i,j}}{\partial p_l} \tag{12}$$

$$i = 1,2,\cdots,nr\ ;\ j = 1,2,\cdots,ns\ ;\ l = 1,2,\cdots,N\ .$$

Note that the imaginary part of equation (12) is $\frac{\partial \tau_{i,j}}{\partial p_l}$ multiplied by $\omega$. By dividing the partial derivative wavefield by the forward modeled wavefield (note that we already computed the Fréchet derivative wavefield using the reciprocity theorem), we can extract the Fréchet derivative of the first arrival traveltime with respect to the subsurface velocity parameter.

**Inversion theory**

In the refraction tomography, we update the velocity model by minimizing the $L_2$-norm of residual errors between the first arrival traveltimes of the real data and those of the numerical modeling. The residual error of the traveltime at the n receiver point, $\Delta\boldsymbol{\tau}$ is defined as the difference between the observed traveltime and that of the numerical model. The residual error can be defined as

$$\Delta\tau_{i,j} = (\tau_d)_{i,j} - (\tau_u)_{i,j} \tag{13}$$

$$i = 1,2,\cdots,nr\ ;\ j = 1,2,\cdots,ns$$

where the subscript denotes the individual components of $\Delta\boldsymbol{\tau}$, $\boldsymbol{\tau}_\mathbf{d}$ and $\boldsymbol{\tau}_\mathbf{u}$, the subscript $i$ represents the receiver number and the subscript $j$ represents the shot number. As is common in many inverse problems, the $L_2$-norm misfit function with respect to the velocity parameter $p_l$ is defined as

$$E(\mathbf{p}) = \frac{1}{2} \Delta\boldsymbol{\tau}^{\mathrm{t}} \Delta\boldsymbol{\tau} \tag{14}$$

where the superscript $\mathbf{t}$ is the transpose.

In general, we can minimize the object function in three different ways (Lines and Treitel, 1984), namely full Newton method, Gauss-Newton method and the steepest descent method. All of these methods require Fréchet derivative to be obtained, either directly or indirectly. In this paper, we choose the steepest descent method. In the steepest descent method, we update a velocity model by following a general iterative rule

$$\mathbf{p}^{(k+1)} = \mathbf{p}^{(k)} - \alpha^{(k)} \nabla_p E^{(k)} \tag{15}$$

where

$$\nabla_p E^{(k)} = \frac{\partial E}{\partial \mathbf{p}} = \mathbf{J}^{\mathbf{t}} \Delta \boldsymbol{\tau} \tag{16}$$

where $k$ is an iteration number, $\nabla_p E^{(k)}$ is the steepest descent direction perpendicular to the objective function at the $k$-th iteration and $\alpha$ is a step length. In equation (16), $\Delta\boldsymbol{\tau}$ is the $(ns \times nr) \times 1$ column vector and the matrix $\mathbf{J}^{\mathbf{t}}$ is the transpose of the $(ns \times nr) \times N$ Jacobian matrix. Since $\boldsymbol{\tau}_{\mathbf{d}}$ is not function of the parameter $p_l$, the elements of Jacobian matrix are given by

$$J_{(j-1)\times nr+i,l} = \frac{\partial \tau_{i,j}}{\partial p_l} \tag{17}$$

$$i = 1,2,\cdots,nr\,;\; j = 1,2,\cdots,ns\,;\; l = 1,2,\cdots,N$$

where the subscript $i$ and $j$ represents the receiver number and the shot number, respectively, and the subscript $l$ represents the parameter number.

Now, we need to determine $\alpha$ to minimize the $L_2$-norm in the direction given by the steepest descent direction, $\nabla_p E^{(k)}$. Using the Gauss-Newton or full Newton method, we can obtain the step length by inverting the full Hessian or an approximate Hessian and multiplying the steepest descent direction by the inverse of the Hessian. However, the computation of the Hessian is a formidable task for even a modern high-tech computer to handle if the number of the unknowns is increased. Furthermore, calculating an inverse of the huge Hessian is also prohibitively expensive(Shin et al. 2001).

Hence, we regularize the steepest descent direction by diagonal approximation of the Hessian. Due to the ill-posedness of the Hessian matrix, we apply a diagonally damped least squares method described by Shin et al.(2001).

## 3. Results

### Verification of Fréchet derivative

To verify the derivative of the traveltime using our algorithm, we have compared the analytically calculated Fréchet derivative with the numerically calculated Fréchet derivative (Lines and Treitel, 1983). By the finite difference formula, the variation of traveltime $\tau_i$ with respect to the parameter $p_j$ is expressed by

$$J_{i,j} = \frac{\partial \tau_i}{\partial p_j} = \frac{\tau_i(p_j + \Delta p_j) - \tau_i(p_j - \Delta p_j)}{2\Delta p_j} \tag{18}$$

The velocity model chosen for verifying Fréchet derivative is shown in Figure 1. The size of this model is 5km in horizontal distance and 0.5km in depth. The velocity of the model is 2km/s. For the calculation of the Fréchet de-

rivative, we subdivide the model into 500×50 elements whose grid size is 10m. We then perturb the element at 0.1km depth point in the middle of the model and measure all traveltimes along the surface.

Figures 2(a), (b), and (c) show the analytic Fréchet derivative and the finite difference Fréchet derivative where the shot position is located at 1.5km, 2.5km, 4.5km, respectively. We note that all the Fréchet derivatives agree with one another almost perfectly.

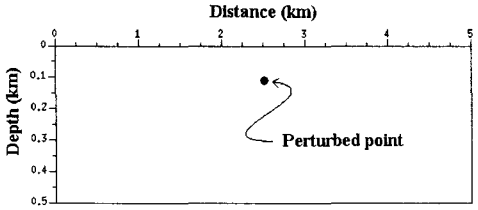


Figure 1. Velocity model for comparing the analytic Fréchet derivative with the numerical Fréchet derivative.

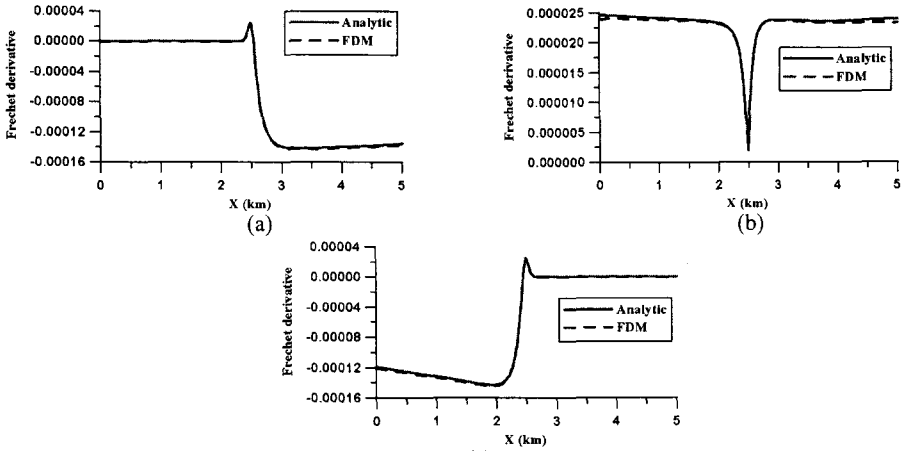


Figure 2. Comparison between the analytic Fréchet derivative and the numerical Fréchet derivative where the shot is located at (a) 1.5km, (b) 2.5km, (c) 4.5km, respectively.

## An isolated block embedded in the two-layered model

To calibrate our algorithm, we have inverted an isolated block embedded in the two-layered model. Figure 3(a) shows the true model. The velocity of the first layer is 1.5km/s, the velocity of the second layer is 4.5km/s and the velocity of the block in the middle is 3km/s. The size of this model is 3km in horizontal distance and 0.5km in depth. The initial model is the linearly increasing velocity model with a depth ranging from 1.5km/s to 3.5km/s, as shown in Figure 3(b). We subdivide the velocity model into 301×51 elements. Three hundred and one receivers are placed on the surface at 10m intervals.

Figure 3(c) displays the inverted model at 600-th iteration. From Figure 3(c), we note that the inverted velocity model converges to the true model. Figure 4(a) shows the rms error of the traveltime, which reaches up to 10% of the initial error at 200 iterations and to about 1.7% at 600 iterations.

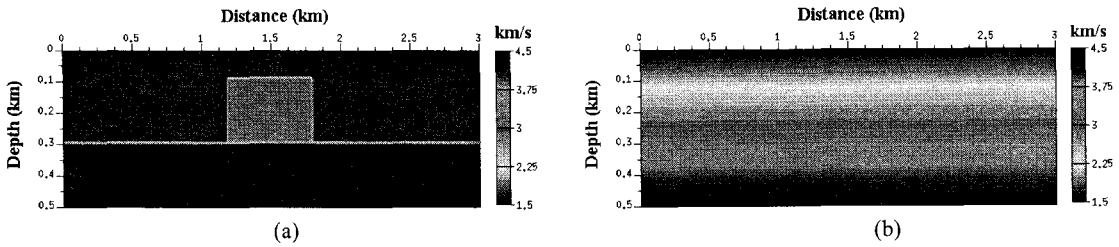

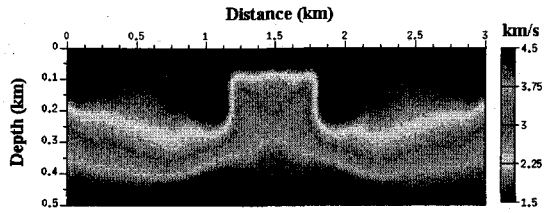


(c)

Figure 3. (a) An isolated block embedded in the two-layered model, (b) the initial model for the inversion and (c) the last inverted model.

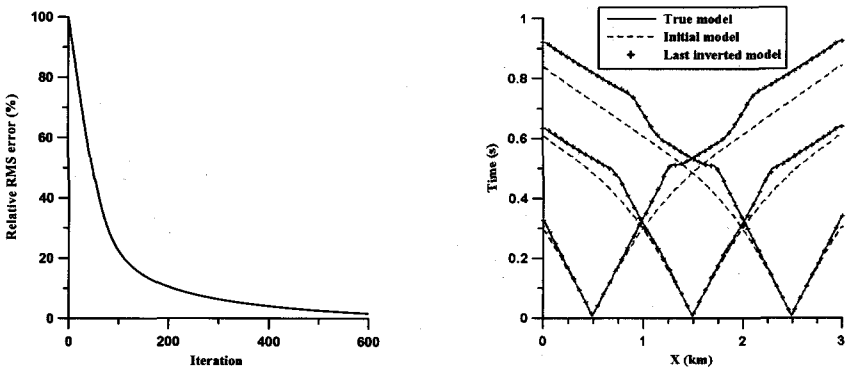


(a) (b)

Figure 4. An isolated block embedded in the two-layered model : (a) The history of RMS error of our inversion results and (b) the traveltime curves of the true model, the initial model and the last inverted model.

## Marmousi-2 model

Having finished a successful inversion of the simple model, we proceed to invert the traveltimes generated for Marmousi-2 model(Martin et al., 2002). Figure 5(a) shows the P-wave velocity-depth model of Marmousi-2 model. For simplicity, we peeled off a layer of water of Marmousi-2 model. The horizontal distance of this model was 17km and the depth, 3km. The lowest velocity was 1.028 km/s mainly in the gas charged sand channel and gas sand trap and the maximum velocity is 4.7km/s in the salt layer. The initial model for inverting Marmousi-2 model is shown in Figure 5(b). The velocity of the surface is 1.5km/s and the velocity is seen to increase linearly as the depth increases. The velocity at 3km in depth is 4.5km/s. Eight hundred and fifty one shots are located on the surface at intervals of 20m. The same number of receivers for each shot are located on the surface at 20m intervals.

Figure 5(c) shows the inversion result at 200-th iteration. The faults at the middle of the model are vaguely defined but the structure of the shallow subsurface approximates to the true model. Figure 6(a) shows the rms error of the traveltime for Marmousi-2 model. The rms error of the traveltime decreases by about 6.6% of the initial error at 200 iterations. Figure 6(b) represents the traveltime curves for the true, the initial and the last inverted model, respectively, where the shot position is located at 2km, 8.5km, and 15km. The traveltime curve obtained from the last inverted model shows good agreement with those obtained from the true model.

To verify whether the inverted velocity-depth model can be used for smooth velocity model for the prestack depth migration, we applied Kirchhoff prestack depth migration using the most energetic traveltime(Shin et al, 2003) for the Marmousi model. Figures 7(a), (b), and (c) show the Kirchhoff migrated images by using the true, the initial and the last inverted velocity model, respectively. We note that the image migrated using the inverted velocity model is improved much more than the image using the initial velocity model. Especially, the depth of the left part is observed to have improved considerably, the outline of the faults in the middle is well defined and the continuity of the anticline in deeper area is enhanced.

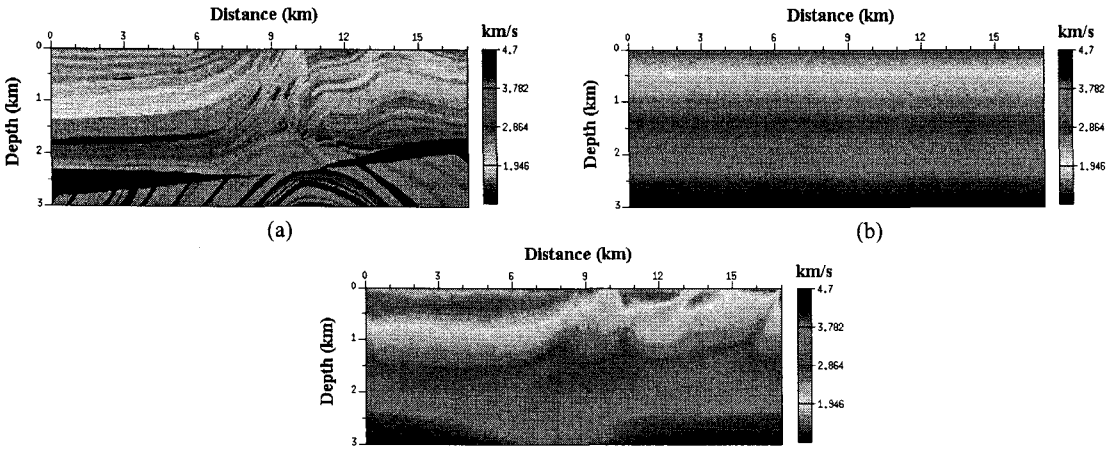


Figure 5. (a) Marmousi-2 model, (b) the initial model for the inversion and (c) the last inverted model.

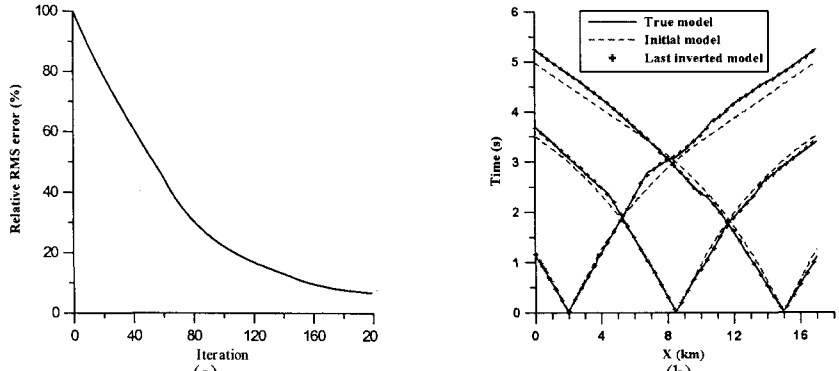


Figure .6 Marmousi-2 model : (a) The history of RMS error of our inversion result and (b) the traveltime curves of the true model, the initial model and the last inverted model.

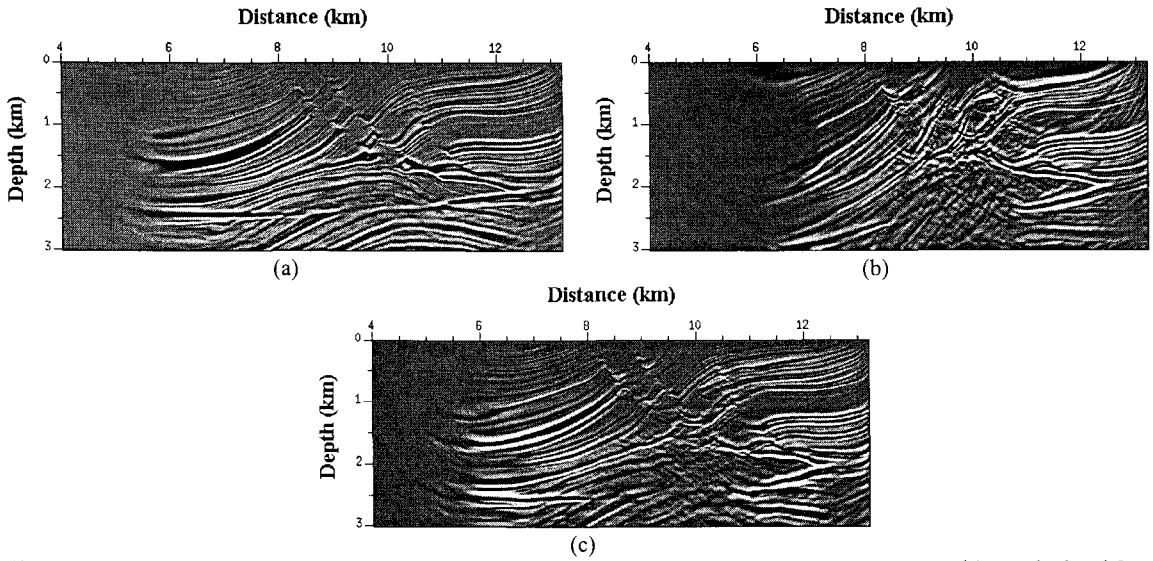


Figure 7. Kirchhoff prestack depth images for the Marmousi-2 model by using the most energetic traveltime calculated from (a) the true model, (b) the initial model and (c) the last inverted model.

## 4. Conclusions

By combining the damped wave solution in frequency domain with the reciprocity theorem of wave equation, we proposed a new technique for calculating the traveltimes and their Fréchet derivatives with respect to the subsurface parameter such as velocity. Our algorithm enables us to construct the diagonal elements of the approximate Hessian, thereby allowing us to obtain a better-scaled step length than the steepest descent direction without any regularization.

Instead of showing examples of the inversion of the traveltimes for the shallow subsurface, we applied our algorithm to Marmousi-2 model to obtain the smooth velocity model for the prestack depth migration. In our test, we assumed that we could locate shots and receivers at every grid point on the surface. Through our numerical test of Marmousi-2 model, the refraction tomography with large aperture data can be used to build the smooth velocity model for the prestack Kirchhoff migration as well as to obtain the velocity model of the shallow subsurface.

The extension of our algorithm to calculation of Fréchet derivative of the absolute amplitude of the first arrival event is straightforward, thus allowing us to include the amplitude term in the refraction tomography. With the implementation to the amplitude term to the refraction tomography, we believe that we can extend our algorithm to transmission tomography without any difficulty.

## Acknowledgement

This work was funded by the National Laboratory Project of the Ministry of Science and Technology and under the grant of the Brain Korea 21 project of the Ministry of Education.

## References

Docherty, P., 1992, Solving for the thickness and velocity of the weathering layer using 2-D refraction tomography: Geophysics, 57, 1307-1318.

Hampson, D., and Russell, B., 1984, First break interpretation using generalized linear inversion: 54th Ann. Internat. Mtg., Soc. Expl. Geophys., Expanded Abstracts, 532-534.

Landa, E., Keydar, S., and Kravtsov, A., 1995, Determination of shallow velocity-depth model from seismic refraction data by coherency inversion: Geophys. Prosp., 43, 177-190.

Lines, L.R., and Treitel, S., 1984, Tutorial: A review of least-square inversion and its application to geophysical problems: Geophys. Prosp., 32, 159-186.

Marfurt, K. J., 1984, Accuracy of finite-difference and finite-element modeling of the scalar and elastic wave equations: Geophysics, 49, 533-549.

Martin, G. S., Marfurt, K. J., and Larsen, S., 2002, Marmousi-2: an updated model for the investigation of AVO in structurally complex areas: 72nd Ann. Internat. Mtg., Soc. Expl. Geophys., Expanded Abstracts, 1979-1982.

Shin, C., 1988. Non-linear elastic wave inversion by blocky parameterisation: Ph.D. thesis, Univ. of Tulsa.

Shin, C., Ha, J., and Jeong, S., 1999, Refraction tomography by blocky parameterisation: Journal of Seismic Exploration, 8, 143-156.

Shin, C., Jang, S., and Min, D., 2001, Improved amplitude preservation for prestack depth migration by inverse scattering theory: Geophys. Prosp., 49, 592-606.

Shin, C., Yoon, K., Marfurt, K. J., Park, K., Yang, D., Lim, H., Chung, S., and Shin, S., 2001, Efficient calculation of a partial-derivative wavefield using reciprocity for seismic imaging and inversion: Geophysics, 66, 1856-1863.

Shin, C., Ko, S., Kim, W., Min, D., Yang, D., Marfurt, K. J., Shin, S., and Yoon, K., 2003, Traveltime calculations from frequency domain downward continuation algorithms: Geophysics online.

Shin, C., Ko, S., Marfurt, K. J., Yang, D., 2003, Wave equation calculation of most energetic travel times and amplitudes for Kirchhoff prestack migration: Submitted to Geophysics.